MDPI

Article

Polyhedral Effects on the Mass Activity of Platinum Nanoclusters

Forrest H. Kaatz [1,*] and Adhemar Bultheel [2]

[1] Mesalands Community College, 911 South 10th Street, Tucumcari, NM, 88401, USA
[2] Dept. Computer Sci., KU Leuven, Celestijnenlaan 200A, 3001 Heverlee, Belgium
* Correspondence email: fhkaatz@gmail.com

Version August 24, 2020 submitted to Catalysts

Abstract: We use a coordination-based kinetics model to look at the kinetics of the turnover frequency (TOF) for the oxygen reduction reaction (ORR) for platinum nanoclusters. Clusters of octahedral, cuboctahedral, cubic, and icosahedral shape and size demonstrate the validity of the coordination-based approach. The Gibbs adsorption energy is computed using an empirical energy model based on density functional theory (DFT), statistical mechanics, and thermodynamics. We calculate the coordination and size dependence of the Gibbs adsorption energy and apply it to the analysis of the TOF. The platinum ORR follows a Langmuir-Hinshelwood mechanism, and we model the kinetics using a thermodynamic approach. Our modeling indicates that the coordination, shape, and the Gibbs energy of adsorption all are important factors in replicating an experimental TOF. We investigate the effects of size and shape of some platinum polyhedra on the oxygen reduction reaction (ORR) and the effect on the mass activity. The data is modeled quantitatively using lognormal distributions. We provide guidance on how to account for the effects of different distributions due to shape when determining the TOF.

Keywords: catalysis; reaction kinetics; coordination; nanoclusters; platinum

1. Introduction

There is a long history of speculation that catalytic reactions depend on structure and shape and thus the coordination of the catalyst [1]. Indeed, in 1985, Falicov and Somorjai, proposed coordination sensitive edge and kink sites would be most likely to be active for structure sensitive reactions [2]. Nanocluster synthesis has reached the stage where narrow particle size distributions of desired shapes of many elements and alloys may be achieved [3]. This allows experimentalists to fine-tune catalytic reactions so that specific shapes, sizes, and thus the coordination of the catalyst is known. We model the kinetics (turnover frequency, TOF) of surface sites showing that they strongly depend on the shape and structure of nanoclusters.

The oxygen reduction reaction (ORR) has much application to fuel cell technology. There is previous work on the size dependence of the ORR. Shao, et al. showed experimentally in 2011 that platinum nanoparticles have a maximum in the mass activity around 2.2 nm [4]. Likewise, there have been modeling efforts by Nesselberger et al. [5], Tritsaris et al. [6], and Tripkovic, et al. [7]. Somewhat more recently, Rück, et al. have determined the platinum ORR size dependence via density functional theory (DFT) [8]. Also DFT has been combined with kinetic Monte Carlo methods to look at the TOF on platinum nanoclusters [9]. We calculate the Gibbs energy using an established procedure [10] for the ORR reactions and incorporate it into the mass activity of the ORR via the TOF. This may lend insight into experimental needs of cluster morphology and its impact on the TOF.

Recently, we have determined coordination specific magic formulas for the surface sites of 19 different nanoclusters [11,12]. These magic formulas can assist our understanding of the coordination

and size dependent surface behavior of clusters. In the size dimension of the mesoscale, neither the atomic nor bulk apply, and much activity relies on the surface coordination of the specific cluster being studied. While the exact dimensions of the mesoscale are ambiguous, a good approximation is clusters with diameter $D \sim 5 - 100$ nm. DFT studies on the surface states of nanoclusters show that for $D \sim 3$ nm for gold [13], and about $D \sim 2$ nm, for platinum [14], the transition from the atomic to bulk has occurred. In addition, Hoover, et al. calculate that the difference in entropy between the thermodynamic prediction and the exact entropy is less than k_B (Boltzmann's constant) when the number of atoms, $N > 400$ for classical close packed harmonic cubes [15]. This shows that quite small clusters may be modeled with thermodynamics. Similarly, an estimate of D as a lower limit of the mesoscale can be made from thermal fluctuations [16]. For a cube of dimension D and volume D^3, with ρ_n atoms per unit volume, the thermal fluctuations are about $\delta T/T \approx (\rho_n D^3)^{-1/2}$. For solids and liquids, $\rho_n \approx 50/\text{nm}^3$. If we accept fluctuations of 10^{-2}, this gives $D \approx 5$ nm.

The Gibbs adsorption energy has been calculated by a few authors using a DFT approach [17,18]. Unfortunately, the size range of interest for the TOF is rather large for DFT, and a range of sizes is required. We provide a coordination approach using an empirical energy model combined with DFT, and add statistical mechanics along with thermodynamics to complete the Gibbs adsorption energy calculation. This enables us to determine the Gibbs adsorption energy, ΔG as a function of size and coordination. By modeling clusters using a coordination approach, we are able to avoid the need for supercomputer calculations, as the computational demands are modest (only desktop models required). This is a different approach to calculating the Gibbs energy.

2. Methods

We define G as the Gibbs energy of the cluster (which depends on the size), then because of adatoms being bonded to the outer shell atoms there is an increase in G that is called the adsorption energy and is denoted as ΔG. This can be split up over different coordination types of the atoms on the outer shell bonding to adatoms. We suppose a kink atom adds to the adsorption energy with an amount ΔG_k. Similarly an edge atom adds ΔG_e, while a facet atom contributes ΔG_f then [19]:

$$\Delta G = \sum_{o \in \{f,e,k\}} \Delta G_o N_o \tag{1}$$

where N_o is the number of atoms in the outer shell of the indicated type. If $N_S = N_f + N_e + N_k$ is the total number of atoms in the outer shell bonded to adatoms, then this can be rewritten as:

$$\Delta G = \Delta G_f \cdot (1 - f_e - f_k) + \Delta G_e \cdot f_e + \Delta G_k \cdot f_k \text{ where } f_o = N_o/N_S, \ o \in \{f,e,k\}, \tag{2}$$

where the edge and kink sites which have explicit coordinations for specific structures - see Table 1. Note that equation (2) applies to adsorption to on-top sites, otherwise not all adatoms will be bonded to atoms in the outer shell.

Table 1. Formulas for nanocluster shapes [11,12]. The variable n refers to the number of shells in the cluster, cn to standard coordination number, fcc to face centered cubic, N_S the number of surface atoms, and N_T the total number of atoms.

cn	fcc Truncated Cube	cn	fcc Octahedron
5	$12n-12$	4	6
7	24	7	$12n-12$
8	$12n^2-12n-18$	8	$4n^2-12n+8$
N_S	$12n^2-6$	N_S	$4n^2+2$
N_T	$4n^3+3n^2+3n-7$	N_T	$\frac{2}{3}n^3+2n^2+\frac{7}{3}n+1$
cn	Icosahedron	cn	fcc Cuboctahedron
6	12	5	12
8	$30n-30$	7	$24n-24$
9	$10n^2-30n+20$	8,9	$6n^2-12n+6, 4n^2-12n+8$
N_S	$10n^2+2$	N_S	$10n^2+2$
N_T	$\frac{10}{3}n^3-5n^2+\frac{11}{3}n-1$	N_T	$\frac{10}{3}n^3-5n^2+\frac{11}{3}n-1$

We have a fundamental relationship for the Gibbs energy and adsorption constant, K_a:

$$K_a = \exp\left(-\frac{\Delta G}{RT}\right), \tag{3}$$

where R is the gas constant and T is the temperature in Kelvin. Brønsted-Evans-Polanyi relationships are widely used in homogeneous and heterogeneous catalysis [19,20] using a relationship for reaction constants k and equilibrium constants K as follows:

$$k = gK^{\alpha}, \quad 0 < \alpha < 1, \tag{4}$$

where g and α (Polanyi parameter) are constants. The Polanyi parameter is unitless and a proper fraction, as given originally by Brønsted [21]. We then have:

$$k_a = k'_a \exp\Big(-\alpha\big(f_n^e \cdot \chi_e(D_n) + f_n^k \cdot \chi_k(D_n)\big)\Big), \tag{5}$$

where

$$\chi_e(D) = \frac{\Delta G_e(D) - \Delta G_f(D)}{RT}, \quad \chi_k(D) = \frac{\Delta G_k(D) - \Delta G_f(D)}{RT}, \tag{6}$$

and

$$k'_a = g\exp\left(-\alpha\frac{\Delta G_f}{RT}\right). \tag{7}$$

We now proceed with the explanation of the method to calculate ΔG.

In the early 1990's, DFT studies on metal clusters gave $E(cn_i)$, the bonding energy of atom i, as a function of its coordination cn_i, and that led to the following empirical relationship [22]:

$$E(cn_i) = E_0 - A\cdot\sqrt{cn_i} + B\cdot(cn_i), \tag{8}$$

where E_0, A, and B are constants of the fit [10]. By definition, we then have the bond energies, E_{ij} as a function of coordination:

$$E_{ij} = \frac{1}{2 \cdot cn_B} \left(E(cn_i) + E(cn_j) \right), \tag{9}$$

where cn_B is the bulk coordination, or 12 for fcc metals. For details on this model, we refer the reader to reference [10].

Table 2. Bond strength parameters for platinum, where R^2 is the least squares regression.

Element	E_0	A	B	R^2
Pt	0.0	1.7898	0.0501	0.987

To allow for small deviations from the average bond length, we define i and j as nearest neighbors, and separate them from the rest by requiring that $r_{ij} < r_c$ where r_c is a threshold value, appropriate for the nanocluster. The value for r_c must be less than the distance for second nearest neighbors and varies with the crystal structure. For fcc crystals, $r_c < 1.41 \cdot r_{min}$, where r_{min} is the smallest bond length [12]. Thus,

$$\mathbf{A}(i,j) = \begin{cases} 1, \text{ if } r_{ij} < r_c \text{ and } i \neq j \\ 0, \text{ otherwise} \end{cases} \tag{10}$$

describes the adjacency matrix for the cluster, and

$$\mathbf{E}(i,j) = \begin{cases} r_{ij}, \text{ if } r_{ij} < r_c \text{ and } i \neq j \\ 0, \text{ otherwise} \end{cases} \tag{11}$$

describes the Euclidean matrix for the cluster. We use an adjacency matrix and Euclidean matrix to determine the diameter, D, of the nanoclusters [11], where the bond length in the clusters depends on the average coordination [23]:

$$r(cn) = \frac{2r_B}{\left(1 + \exp\left(\frac{12 - \langle cn \rangle_c)}{8 \cdot \langle cn \rangle_c}\right)\right)}. \tag{12}$$

Here r_B is the bulk bond length and $\langle cn \rangle_c$ is the average coordination of the cluster. We find a linear relationship between D and n, the number of cluster shells, as shown in Table 3:

$$D(n) = a \cdot r_B \cdot n + b. \tag{13}$$

This relationship is derived from MATLAB code for calculating the cluster diameter.

Table 3. Linear constants for $D(n)$.

a	b	Nanocluster
1.722	0.2944	Pt Truncated Cube
1.414	0.0239	Pt Cuboctahedron
1.0	0.0282	Pt Octahedron
2.0	0.0273	Pt Icosahedron

The energies of adsorbates have been shown to scale linearly with generalized coordination [24,25]. We use a DFT model for energies of adsorbates [24]:

$$\overline{CN}_i = \sum \frac{cn_j \cdot n_j}{cn_{\max}} \tag{14}$$

where the sum is over all nearest neighbors of i, $cn_{\max} = 12$ for top sites, 18 for bridge sites and has other values for other types of sites [24]. In this equation n_j is the number of nearest neighbors, hence

each neighbor j of atom i has a weight of n_j/cn_{max} associated with the site. Adsorbate energy, E_{ad}, is linear with generalized coordination [24]:

$$E_{ad} = \overline{CN}_0 + m \cdot \overline{CN}_i. \tag{15}$$

Table 4 shows the values of the linear fits as determined by equation (15).

Table 4. Linear fit of E_{ad} for adsorption.

species	$\overline{CN}_0$ (eV)	slope m of E_{ad} vs $\overline{CN}_i$
Pt-O_2 [24]	−2.418	0.227
Pt-H* [26]	−0.3405	0.0562

We construct our cluster-adatom Hamiltonian as follows:

$$\mathbf{H}(i,j) \approx \begin{cases} E_{ij} & i,j \text{ in the nanocluster} \\ E_{ad} & \text{for an adatom bond} \\ 0 & \text{otherwise} \end{cases} \tag{16}$$

with only nearest neighbor non-zero entries, i.e. a sparse matrix. In the Hamiltonian approach, the partition function is [10,27,28]:

$$Z = \text{Tr}\, e^{-\beta \mathbf{H}} \tag{17}$$

and $\beta = 1/k_B T$ is the inverse temperature, where k_B is Boltzmann's constant, T is the temperature in Kelvin (we use T = 300K), Tr is the trace of the following matrix, and $\mathbf{H}$ is the Hamiltonian matrix, as given by equation (16) [10]. The probability of each state is then $p_j = e^{\beta \lambda_j}/Z$, where Z is the partition function, equation (17), and λ_j is an eigenvalue of the Hamiltonian matrix [28].

The Gibbs energy of adsorption in the nanoscale systems we examine is in joules (J), if we neglect the small PV (pressure - volume) term, [10,27]

$$\Delta G = -RTN_n \ln Z, \tag{18}$$

where Z is the partition function, equation (17) and where $N_n = N_c + N_\theta$, with N_c the number of atoms in the cluster and N_θ the number of adatoms at coverage theta. The Gibbs adsorption energy here is converted from more standard units by dividing by N_θ and using a conversion factor (R/k_B) to get units of (J/mol). We average several times over the nanocluster system, since especially for the kink sites, the statistics are low.

3. Results and Discussion

3.1 Langmuir-Hinshelwood Mechanism

In general, the TOF for reactions may display structure sensitivity which rises or decreases with size, or is not sensitive, or passes through a maximum [29]. The literature discusses several types of reactions, including a Two-Step sequence and its corollary, the Eley-Rideal reaction, and the Langmuir-Hinshelwood (L-H) mechanism [30]. The L-H mechanism is relevant for surface reactions [31]:

$$\begin{array}{ll} 1. & \text{A + Z} \leftrightarrow \text{ZA} \quad \text{(quasi - equilibrium)} \\ 2. & \text{B + Z} \leftrightarrow \text{ZB} \quad \text{(quasi - equilibrium)} \\ 3. & \text{ZA + ZB} \rightarrow \text{C + 2Z} \end{array} \tag{19}$$

$$\text{A + B} \rightarrow \text{C}$$

where A and B are reactants, C is the product, and Z is a surface site. The reaction rate is [30]

$$v(D) = \frac{k_3 K_1 P_A K_2 P_B}{(1 + K_1 P_A + K_2 P_B)^2}, \tag{20}$$

where we have

$$K_1(D) = K_A \exp\left\{-\left(f_e \cdot \chi_e^A(D) + f_k \cdot \chi_k^A(D)\right)\right\}, \tag{21}$$

$$K_2(D) = K_B \exp\left\{-\left(f_e \cdot \chi_e^B(D) + f_k \cdot \chi_k^B(D)\right)\right\}, \tag{22}$$

where k_3 is the reaction rate constant for sequence 3 (see (19)), P_A and P_B are partial pressures or concentrations (for liquids) of A and B, and for reaction 3 we have

$$k_3(D) = K_C \exp\left\{(1-\alpha)\left[f_e \cdot \left(\chi_e^A(D) + \chi_e^B(D)\right) + f_k \cdot \left(\chi_k^A(D) + \chi_k^B(D)\right)\right]\right\}. \tag{23}$$

After some simplification we get

$$v(D) = \frac{p_1 \exp\left\{(-\alpha)\left[f_n^e \cdot \left(\chi_e^A(D_n) + \chi_e^B(D_n)\right) + f_n^k \cdot \left(\chi_k^A(D_n) + \chi_k^B(D_n)\right)\right]\right\}}{[1 + p_2 \exp\{-[f_n^e \chi_e^A(D_n) + f_n^k \chi_k^A(D_n)]\} + p_3 \exp\{-[f_n^e \chi_e^B(D_n) + f_n^k \chi_k^B(D_n)]\}]^2} \tag{24}$$

where p_1 is a frequency and p_2, p_3 are related to the rate constants and partial pressures of A and B [19,30]. Here, n refers to the dependence on complete shells of nanoclusters. Since we are not aware of other analysis of the data, we use α and the p_i as adjustable parameters. In principle, there are more experimental parameters (Polanyi parameter, kinetic constants, and partial pressures or concentrations) depending in a complicated way on the analysis than we use to model the data. We find that α affects the full width half maximum, FWHM, p_1 affects the peak intensity, and p_2, p_3 affect the center of the peak position.

3.2 Pt ORR

For modeling the platinum mass activity, we assume the O_2 and H* react in a Langmuir-Hinshelwood mechanism, (see (19)), and separate the kink, edge and facet bonding as shown in Figure 1, below. We use platinum polyhedra of icosahedra, cuboctahedra, truncated cubes, and octahedra in our modeling.

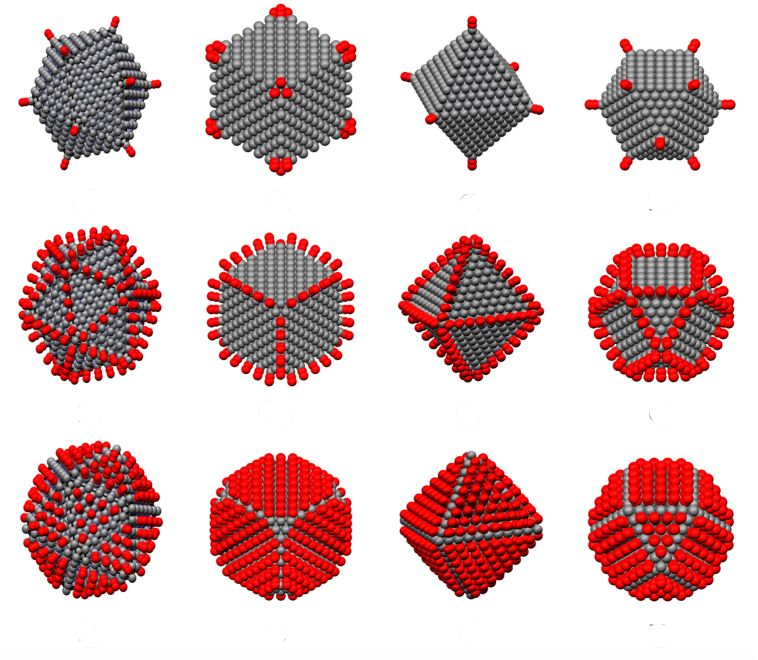

Figure 1. Kink (row 1), edge (row 2) and facet (row 3) bonding of O_2 to platinum clusters.

The ORR follows a L-H mechanism [4] as shown in (25):

$$\begin{array}{ll} 1. & O_2 \rightarrow 2O_{ads} \\ 2. & H_2 \rightarrow 2H_{ads} \\ 3. & 2H_{ads} + O_{ads} \rightarrow H_2O \\ & \\ & 2H_2 + O_2 \rightarrow 2H_2O \end{array} \tag{25}$$

so that in the general scheme of equation (19) above A is O_2 and B is H_2. We also assume the Polanyi constants are equal. We calculate the corresponding χ_e and χ_k as used in the TOF from equation (24), for the various polyhedra as shown in Figure 2 below.

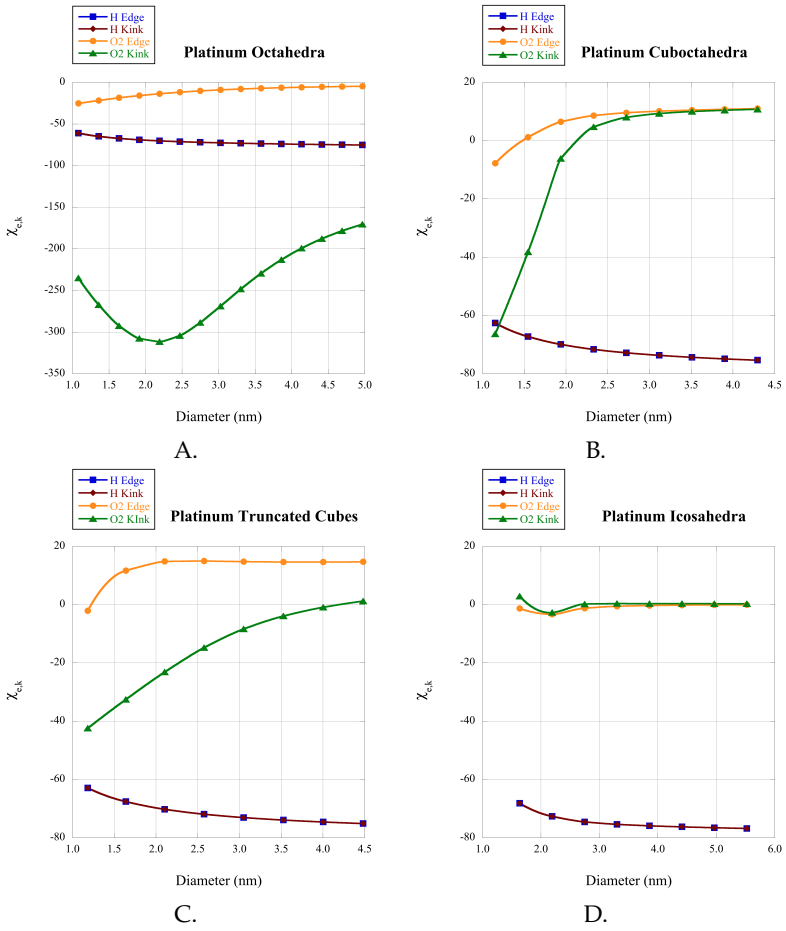

Figure 2. Plots of χ_e and χ_k versus D for the four polyhedra. In all four plots, the data for H-Edge and H-Kink overlap on the scale presented.

The mass activity is basically the product of the dispersion and the TOF [32]

$$MA_{Pt} = \frac{\mathcal{F}}{AW_{Pt}} \frac{N_S}{N_T} \frac{v(D)}{10^3} \quad (\mathrm{A/mg_{Pt}}) \tag{26}$$

where $\mathcal{F}$ is the Faraday constant, 96,485 C/mol and AW_{Pt} is the atomic weight of platinum, 195.08 g/mol. In principle, this gives an exact form of the mass activity, but the kinetic constants and corresponding concentrations are not completely known. We use α and the p_i as modeling parameters and optimize the mass activity for the various clusters. We are not aware of previous modeling of the mass activity using the TOF, or equation (26).

In the original paper on the experimental data of the mass activity for platinum clusters, it was assumed that the nanoclusters had cuboctahedral shape [4]. In Figure 3A, we plot the mass activity versus D for cuboctahedra. The modeled tail of the distribution decays more rapidly than the experimental data. This tells us that the cuboctahedral modeling has a narrower distribution than that observed experimentally. However, if we presume that the experimental mass activity is composed of multiple components from several polyhedra and that the sum from the convolution of the component polyhedra results in an approximation of the experimental curve, we get Figure 3B. Here we model the data with a lognormal distribution with parameters as tabulated in Table 5, while the polyhedra are approximated by cubic splines.

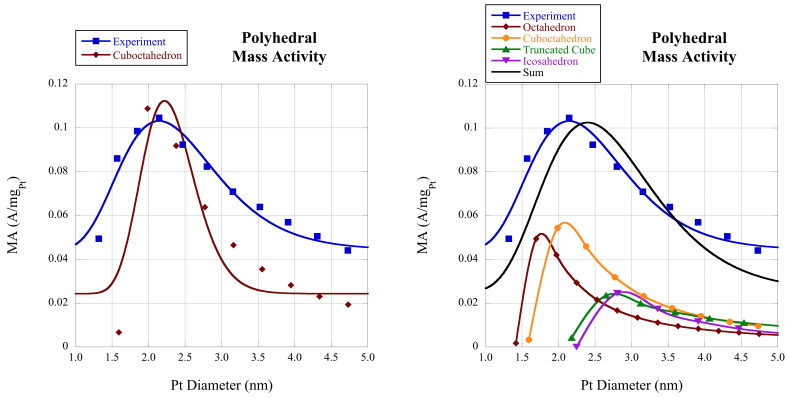

A. B.

Figure 3. A. Mass activity for cuboctahedra. B. Mass activity versus D for adsorption on platinum polyhedra.

Table 5. Mean, $\overline{\mu}$, and standard deviation, $\overline{\sigma}$, for the platinum ORR mass activity for Figure 3, using a lognormal distribution.

Structure	$\overline{\mu}$	$\overline{\sigma}$
Exp Fit	2.46	0.77
Cuboctahedron Fig. 3A	2.31	0.38
Sum Fig. 3B	2.77	0.88

To account for several shapes with independent distributions, we sum over the morphology:

$$v(D) = \sum_i \rho_i \cdot v_i(D), \tag{27}$$

where i is one of the four shapes, octahedra, cuboctahedra, truncated cube, or icosahedra. The shape parameters for the platinum TOF are shown in Table 6.

Table 6. Shape parameters for the platinum TOF via the L-H mechanism.

Structure	α	p_1	p_2	p_3
Octahedron	0.05	$1.0e-10$	$1.0e-13$	$1.0e-13$
Truncated Cube	0.05	$5.0e-2$	$5.0e-7$	$5.0e-7$
Icosahedron	0.05	$1.0e-2$	$1.0e-18$	$1.0e-18$
Cuboctahedron Fig. 3A	0.05	$5.0e-2$	$1.0e-10$	$1.0e-10$
Cuboctahedron Fig. 3B	0.05	$2.5e-2$	$1.0e-10$	$1.0e-10$

If the assumption that the experimental platinum mass activity comes from cuboctahedra is valid, then the calculated curve in Figure 3A is what we find using these procedures. However, if we assume all the polyhedra contribute to the convolution of the experimental curve, good agreement is found for the platinum mass activity for the four polyhedra considered, Figure 3B. The L-H mechanism represents the TOF for platinum nanoclusters fairly well.

Alternatively, the mass activity may be calculated using a kinetic model [7] as:

$$MA_{Pt} = j_s \cdot A_{sp}, \;\; j_s = \sum_f j_f \cdot \exp(-\Delta G_f^a/(k_B T)), \;\; A_{sp} = A_s/m_p = \frac{A_s \cdot N_A}{AW_{Pt} \cdot N_T}, \tag{28}$$

where j_f is 96 and 83 mA/cm^{-2} for (111) and (100) surfaces, respectively, N_A is the Avogadro number, and $\Delta G_f^a = 0.10$ eV or 0.12 eV, for (111) or (100) surfaces respectively, is the DFT calculated free energy barrier for ORR at 0.9 V.

Table 7. Surface area A_s for the polyhedra, where r_B is the bond length for platinum.

Structure	A_s
Octahedron	$2\sqrt{3} \cdot (n \cdot r_B)^2$
Truncated Cube	$12(n \cdot r_B)^2$
Icosahedron	$5\sqrt{3}(n \cdot r_B)^2$
Cuboctahedron	$(6 + 2\sqrt{3}) \cdot (n \cdot r_B)^2$

The specific activity, SA, of single crystal surfaces is known [5], however modeling the SA based on specific surface orientations and the surface dispersion is problematic since assumptions need to be made with respect to the non-contribution of edge and kink sites. In general, the SA follows a trend of facet dispersion [4]. The specific activity is defined as follows:

$$SA = \sum_{o \in \{f,e,k\}} f_o \cdot \mathrm{SA}_{\mathrm{Pt(hkl)}} \quad (\mathrm{mA/cm^2_{Pt}}) \tag{29}$$

where $\mathrm{SA}_{\mathrm{Pt(hkl)}}$ comes from single crystal surfaces and f_o from Table 1. If one assumes that the edge and kink sites make a negligible contribution, then the SA follows the facet trend.

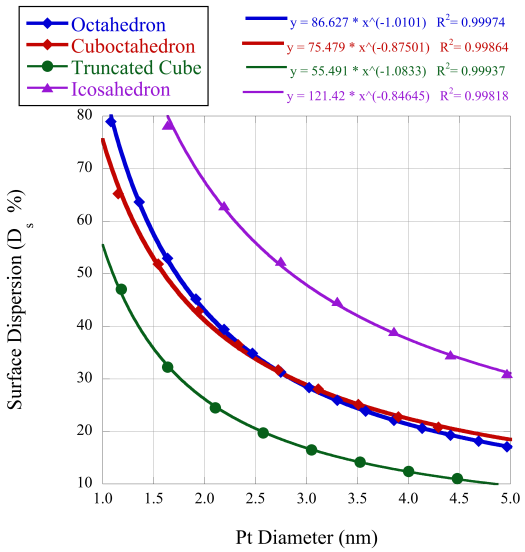

Figure 4. Surface dispersion for the four platinum shapes under consideration.

In Figure 4 above, we plot the surface dispersion $D_s = (N_e + N_k)/N_S \cdot 100\%$ for the four shapes from the equations in Table 1. As can be seen from the data, the surface dispersion is similar for the octahedron and cuboctahedron, and somewhat less for the truncated cube. The icosahedron has a somewhat larger surface dispersion due to the $30n$ factor in the edge sites from Table 1. On the other hand, octahedra have kink sites with coordination $cn = 4$, which is smaller than the other polyhedra.

4. Conclusion

This work represents the computational modeling of the mass activity for the platinum ORR based on a summed contribution of polyhedral distributions. The summed lognormal modeling represents the data reasonably well. These results confirm that coordination, shape, and ΔG have dramatic influence on the catalysis of reactions. The data is made quantitative through modeling with a lognormal distribution. We provided guidance on accounting for different distributions of the TOF based on morphology. We hope these results encourage further experimental work and theoretical modeling. In particular, the Polanyi parameter, the kinetic constants and the partial pressures or concentrations are not known, and these results could in principle lead to a catalytic derivation from fundamental data.

Computational Modeling

All computational modeling uses original code developed by the authors compatible with MATLAB 2020a. Interested readers may contact the corresponding author for details.

Conflict of Interest Statement

Both authors, F.H. Kaatz and A. Bultheel, declare that there is no conflict of interest, financial or otherwise.

Funding

This research did not receive any specific grant from funding agencies in the public, commercial, or not-for-profit sectors.

References

1. Boudart, M. Catalysis by supported metals. *Adv. Catal.* **1969**, *20*, 153–166.
2. Falicov, L.; Somorjai, G. Correlation between catalytic activity and bonding and coordination number of atoms and molecules on transition metal surfaces: Theory and experimental evidence. *Proc. Natl. Acad. Sci.* **1985**, *82*, 2207–2211.
3. Kang, Y.; Pyo, J.B.; Ye, X.; Diaz, R.E.; Gordon, T.R.; Stach, E.A.; Murray, C.B. Shape- controlled synthesis of Pt nanocrystals: The role of metal carbonyls. *ACS Nano* **2013**, *7*, 645–653.
4. Shao, M.; Peles, A.; Shoemaker, K. Electrocatalysis on Platinum Nanoparticles: Particle Size Effect on Oxygen Reduction Reaction Activity. *Nano Letters* **2011**, *11*, 3714–3719.
5. Nesselberger, M.; Ashton, S.; Meier, J.; Katsounaros, I.; Mayrhofer, K.; Arenz, M. The Particle Size Effect on the Oxygen Reduction Reaction Activity of Pt Catalysts: Influence of Electrolyte and Relation to Single Crystal Models. *Am. Chem. Soc.* **2011**, *133*, 17428–17433.
6. Tritsaris, G.; Greeley, J.; Rossmeisl, J.; Nørskov, J.K. Atomic-Scale Modeling of Particle Size Effects for the Oxygen Reduction Reaction on Pt. *Catal. Lett.* **2011**, *141*, 909–913.
7. Tripkovic, V.; Cerri, I.; Bligaard, T.; Rossmeisl, J. The Influence of Particle Shape and Size on the Activity of Platinum Nanoparticles for Oxygen Reduction Reaction: A Density Functional Theory Study. *Catal. Lett.* **2014**, *144*, 380–388.
8. Rück, M.; Bandarenka, A.; Calle-Vallejo, F.; Gagliardi, A. Oxygen Reduction Reaction: Rapid Prediction of Mass Activity of Nanostructured Platinum Electrocatalysts. *Phys. Chem. Lett.* **2018**, *9*, 4463–4468.
9. Jorgensen, M.; Gronbeck, H. Scaling Relations and Kinetic Monte Carlo Simulations To Bridge the Materials Gap in Heterogeneous Catalysis. *ACS Catal.* **2017**, *7*, 5054–5061.
10. Kaatz, F.; Bultheel, A. Catalytic Thermodynamic Model for Nanocluster Adsorbates. *Catal. Today*, in press, **https://doi.org/10.1016/j.cattod.2019.06.077**.
11. Kaatz, F.; Bultheel, A. Magic Mathematical Relationships for Nanoclusters. *Nanoscale Res. Lett.* **2019**, *14*, 150.
12. Kaatz, F.; Bultheel, A. Magic Mathematical Relationships for Nanoclusters - Errata and Addendum. *Nanoscale Res. Lett.* **2019**, *14*, 295.

13. Kleis, J.; Greeley, J.; Romero, N.; Morozov, V.; Falsig, H.; Larsen, A.; Lu, J.; Mortensen, J.; Dułak, M.; Thygesen, K.; Nørskov, J.; Jacobsen, K. Finite Size Effects in Chemical Bonding: From Small Clusters to Solids. *Catal. Lett.* **2011**, *141*, 1067–1071. doi:10.1007/s10562-011-0632-0.
14. Li, L.; Larsen, A.; Romero, N.; Morozov, V.; Glinsvad, C.; Abild-Pedersen, F.; Greeley, J.; Jacobsen, K.; Nørskov, J. Investigation of Catalytic Finite-Size-Effects of Platinum Clusters. *Phys. Chem. Lett.* **2012**, *4*, 222–226.
15. Hoover, W.; Hindmarsh, A.; Holian, B. Number Dependence of Small-Crystal Thermodynamic Properties 1. *J. Chem. Phys.* **1972**, *57*, 1980–1985.
16. Wautelet, M.; Shirinyan, A. Thermodynamics: nano vs. macro. *Pure Appl. Chem.* **2009**, *81*, 1921–1930.
17. Joshi, A.; Tucker, M.; Delgass, W.; Thomson, K. CO adsorption on pure and binary-alloy gold clusters: A quantum chemical study. *J. Chem. Phys.* **2006**, *195*, 194707.
18. Fernandez, E.; Balbas, L. Multiple adsorption of molecular oxygen on small Au/Pd cationic clusters at finite temperature. A van der Waals density functional study. *J. Chem. Phys.* **2016**, *144*, 244308.
19. Murzin, D. Kinetic analysis of cluster size dependent activity and selectivity. *Journal of Catal.* **2010**, *276*, 85–91.
20. Bligaard, T.; Nørskov, J.; Dahl, S.; Matthiesen, J.; Christensen, C.; Sehested, J. The Brønsted–Evans–Polanyi relation and the volcano curve in heterogeneous catalysis. *Journal of Catal.* **2004**, *224*, 206–217.
21. Brønsted, J. Acid and Basic Catalysis. *Chem. Rev* **1928**, *5*, 231–338.
22. Methfessel, M.; Hennig, D.; Scheffler, M. Calculated surface energies of the 4D transition-metals - a study of bond-cutting models. *Appl. Phys. A.* **1992**, *55*, 442–448.
23. Sun, C. Size dependence of nanostructures: Impact of bond order deficiency. *Prog. Solid State Chem.* **2007**, *35*, 1–159.
24. Calle-Vallejo, F.; Martinez, J.; Garcia-Lastra, J.; Sautet, P.; Loffreda, D. Fast prediction of adsorption properties for platinum nanocatalysts with generalized coordination numbers. *Chem. Int. Ed.* **2014**, *53*, 8316–8319. doi:10.1002/anie.201402958.
25. Calle-Vallejo, F.; Tymoczko, J.; Colic, V.; others. Finding optimal surface sites on heterogeneous catalysts by counting nearest neighbors. *Science* **2015**, *350*, 185–189.
26. Pohl, M.; Watzele, S.; Calle-Vallejo, F.; Bandarenka, A. Nature of Highly Active Electrocatalytic Sites for the Hydrogen Evolution Reaction at Pt Electrodes in Acidic Media. *ACS Omega* **2017**, *2*, 8141–8147.
27. Jaynes, E. Information Theory and Statistical Mechanics. *Phys. Rev.* **1957**, *106*, 620–630. doi:10.1103/PhysRev.106.620.
28. Estrada, E.; Hatano, N. Statistical-mechanical approach to subgraph centrality in complex networks. *Chem. Phys. Lett.* **2007**, *439*, 247–251. doi:10.1016/j.cplett.2007.03.098.
29. Strizhak, P. Nanosize effects in heterogeneous catalysis. *Exp. Chem.* **2013**, *49*, 2–21.
30. Murzin, D. Cluster size dependent kinetics: Analysis of different reaction mechanisms. *Catal. Lett.* **2015**, *145*, 1948–1954.
31. Murzin, D. Size-dependent heterogeneous catalytic kinetics. *Mol. Catal. A: Chem.* **2010**, *315*, 226–230.
32. Gasteiger, H.; Markovic, N. Just a dream - or future reality? *Science* **2009**, *324*, 48–49.

© 2020 by the authors. Submitted to *Catalysts* for possible open access publication under the terms and conditions of the Creative Commons Attribution (CC BY) license (http://creativecommons.org/licenses/by/4.0/).